LU-SHENG ZHANG [1], LIU YANG [1], LINGSHENG LI[1]
XIAOYU FENG[1], DE-JU CAO[1], ZHAO-WEN LIU[1, 2]

PHYTOCHELATINS OF *CLADOPHORA RUPESTRIS* IN Pb^{2+} ABSORPTION AND ITS DETOXIFICATION

Phytochelatins (PCs) exist widely in plants and are closely related to plant resistance to heavy metals (HMs). Glutathione (GSH) and nonprotein thiols (NPTs) are the major components of PCs. This study investigates the role of the PCs of *Cladophora rupestris* in Pb^{2+} accumulation and detoxification. The distribution of Pb^{2+} in the PCs of *C. rupestris* was studied. FTIR and XPS are used to characterize the chelating power of Pb^{2+} with PCs in *C. rupestris*. The curve fitting of the secondary protein structure is used to identify the functional groups with Pb^{2+}. Results showed that the content of Pb^{2+} in the PCs of *C. rupestris* increased with an increase in Pb^{2+} stress. Pb content increased to 352 and 314 mg/kg in NPTs and GSH, respectively, when Pb stress concentration reached 7.5 mg/dm^3. The Pb^{2+} fraction of *C. rupestris* PCs reached a maximum of 10.8 and 9.3% in NPTs and GSH, respectively. The Pb^{2+} uptake by GSH and NPTs was 40–48% and 52–60%, respectively. Pb^{2+} bound with the PCs of *C. rupestris*, forming complexes that contained Pb–OOC, Pb–C=O, CO–Pb, –N=Pb, Pb–NH$_2$, Pb–O, Pb–N–, Pb–C–, Pb–S, and Pb^{2+} with multiple groups of PCs as bridging ligand atoms.

1. INTRODUCTION

Heavy metals (HMs) are persistent environmental contaminants that adversely affect the growth and survival of plants [1]. Lead (Pb) is one of the most hazardous pollutants, and it can seriously threaten human health [2]. Phytochelatins (PCs) exist widely in plants and are closely related to plant resistance to HMs. Phytochelate peptides and their complexes comprise a class of low-molecular-weight compounds that are rich in cysteine. PCs such as glutathione (GSH) and nonprotein thiols (NPTs) exhibit

---

[1]Anhui Province Key Laboratory of Farmland Ecological Conservation and Pollution Prevention, School of Resources and Environment, Anhui Agricultural University, Hefei 230036, China, corresponding author D.-J. Cao, email address: cdj@ahau.edu.cn

[2]School of Materials and Environmental Engineering, Chizhou University, Chizhou 247000, China.

strong chelating power on HMs, playing a key role in HM accumulation and detoxification [3]. Fischer et al. [4] studied the response of plants to Pb stress and proved that PCs were involved in the detoxification of Pb. Cd^{2+} and Pb^{2+} could achieve complexation via GSH and PCs [5], with S atoms forming an asymmetric bridge between Pb^{2+} ions [6]. Pb content in *Cladophora rupestris* is correlated with NPTs and GSH, helping this species survive in a Pb-polluted environment [7]. Chen et al. [2] reported that *Chaerophyllum* formed chelates with Pb^{2+} ions.

Many authors studied the detoxification mechanism of HMs by using spectroscopic methods [2, 7, 8]. Cao et al. [9] analyzed the binding state of small molecular organic and functional groups in HMs via Fourier-transform infrared spectroscopy (FTIR). Through FTIR and 3D-excitation-emission matrix fluorescence spectroscopy, they determined that groups such as –OH, –COOH, and –SH, in *C. rupestris* can bind to Pb under the stress of this HM to reduce its toxicity [10]. X-ray photoelectron spectroscopy (XPS) showed that the esterification reaction of dialcohol could significantly improve the adsorption of HMs [11]. *C. rupestris* is widely distributed in water environments; it has important functions in aquatic ecosystems [12]. The roles of *C. rupestris* PCs in Pb accumulation, detoxification, and mechanism remain unclear.

The authors aimed to investigate the roles of *C. rupestris* PCs in Pb^{2+} accumulation and detoxification. The distribution of Pb in *C. rupestris* PCs was studied. FTIR and XPS were used to characterize the chelating power and mechanism of Pb^{2+} with *C. rupestris* PCs. The curve fitting of the protein secondary structure was used to realize the functional groups. This study may reveal the role of plant PCs in addressing HM contamination in the environment.

2. MATERIALS AND METHODS

C. rupestris cultivation and preparation. *C. rupestris* was collected from the surface water of a pond in Hefei, Anhui Province, China (31°50′N, 117°11′E). A bold basal medium (BBM) was used as the culture medium, and the pH was set as 7.5±0.5 [9, 12]. *C. rupestris* was grown in an incubator (SPX-250B-G) at 25 °C, with light intensity ranging from 3000 to 4000 lx (light and dark cycle of 12:12 h). *C. rupestris* was grown in a BBM that contained various concentrations of $Pb(NO_3)_2$. The Pb concentration was 0, 0.5, 1.0, 2.5, 5.0, 7.5, and 10.0 mg/dm^3 and the cultivation time was 7 days.

Extraction of PCs. After 7 days, 0.5 g of *C. rupestris* sample was placed in a mortar. Then, the precooled extraction buffer for fully grinding the homogenate, the precooled 5% (V/V) sulfosalicylic acid with 6.3 $mmol/dm^3$ of pentetic acid (pH < 1), and a small amount of quartz sand were added. Then, the mixture was centrifuged at 10 000 relative centrifugal force (RCF) at 4 °C for 15 min, and the supernatant obtained was the NPT extract [10]. Then 25% ethanol solution was added, stirred in a water bath at 50 °C for

60 min, and centrifuged at 3000 rpm for 10 min. The resulting supernatant was the GSH extract.

Determining the Pb content of PCs. PCs extracted from 0.5 g of *C. rupestris* were added and fully ground in a 50 cm^3 Teflon™ digestion tank. Then, 8 cm^3 of 65% HNO$_3$ was added, and the digestion tank was covered overnight. The mixture was digested at 105 °C for 1.5 h. After the red-brown smoke dissipated, 2 cm^3 of HClO$_4$ was added to continue digestion at 135 °C for about 0.5 h. The digestion residue maintained a constant volume of up to 25 cm^3 with 1% HNO$_3$. Pb content was determined via atomic absorption spectrometry at 283.3 nm.

FTIR and XPS. First, 0.001 g of freeze-dried NPTs, GSH sample, and dried KBr powder were carefully ground in an agate mortar, mixed evenly, pressed with a mold, and placed in the sample tank for determination under the following conditions: test interval 400–4000 cm^{-1}, scanning time 32, and resolution 4 cm^{-1}. The FTIR spectra of GSH and NPT protein amide bands within the range of 1700–1600 cm^{-1} were analyzed through the second derivative. The protein secondary structure was studied via curve-fitting analysis [7].

The sample was placed at −80 °C for 6 h and then freeze-dried. XPS results were analyzed with a Thermo ESCALAB250Xi spectrometer. The excitation source of monochromatized AlKα (*hv* = 1486.6 eV) was used, with passing energy of 30 eV; the positions of the peaks of Ag 3d5/2 (368.21 eV), Au 4f7/2 (83.96 eV), and Cu 2p3/2 (932.62 eV) were used to calibrate the energy scale of the spectrometer's core [2, 13]. Data were analyzed using Peak-Fit 4.1, Jade 6.5, and Origin 8.5.

3. RESULTS AND DISCUSSION

3.1. BIOSORPTION EFFECTS OF Pb^{2+} IN *C. RUPESTRIS* PCS

Pb^{2+} concentration in the PCs of *C. rupestris* cells is shown in Fig. 1. Initially, Pb content increased significantly in NPTs with an increase in Pb^{2+} stress concentration. When Pb^{2+} concentration reached 5.0 mg/dm^3, Pb content in NPTs increased slowly. When the concentration of Pb^{2+} stress concentration reached 10.0 mg/dm^3, Pb content in NPTs increased to 352 mg/kg (Fig. 1a). Pb content in GSH increased rapidly with an increase in Pb^{2+} stress concentration at low concentrations. Pb^{2+} content in GSH increased to 314 mg/kg when Pb stress concentration reached 7.5 mg/dm^3. Then, it remained stable with an increase in Pb^{2+} stress.

The Pb content increased significantly in NPTs and GSH. According to Chen et al. [7], NPTs and GSH in *C. rupestris* increased as Pb^{2+} concentration increased. The results

are consistent with the current study. The percentage of Pb in the total *C. rupestris* cells in NPTs and GSH under different Pb concentration stresses is shown in Fig. 1b.
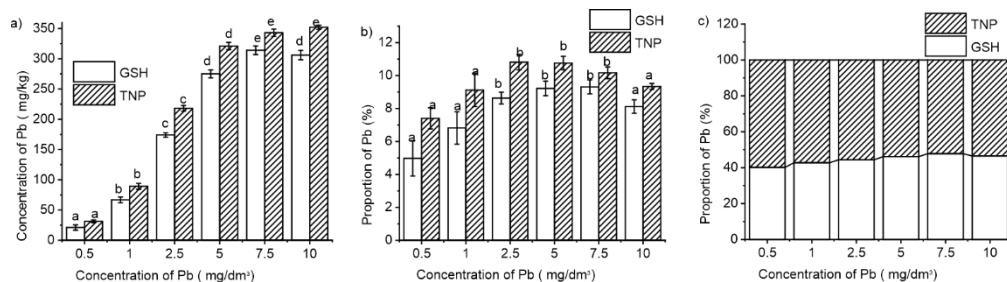

Fig. 1. Contents and proportions of Pb in Phytoehelatins of *C. rupestris*

The percentage of Pb in GSH in the whole cell was 4.9–9.3%, while that in NTP was 7.4–10.8% (Fig. 1b). The proportion of Pb content in the NPTs and GSH of *C. rupestris* increased significantly with an increase in the stress concentration of Pb^{2+}. When Pb^{2+} stress concentration was 2.5 mg/dm³, the Pb^{2+} ratio in NPTs reached a maximum of 10.8%, while that in GSH increased exhibiting a fluctuation trend. $Pb^{2+}$was bound to NPTs, GSH, and PCS [2, 10], and thus, *C. rupestris* PCs play an important role in Pb^{2+} accumulation and detoxification.

A slight difference was observed in the Pb^{2+} accumulation and detoxification of the NPTs and GSH of PCs. The PB uptake by GSH was 40–48% while that of NPT was 52–60.0. Pb^{2+} realized complexation via GSH and PCs [5]. Pb^{2+} penetrated the *Cladophora* cells via the formed chelate between –OH and GSH/metallothionein (MT) [2]. NPTs exhibit strong chelating power on HMs, playing a key role in HM accumulation and detoxification [3].

3.2. MECHANISM OF Pb^{2+} UPTAKE BY *C. RUPESTRIS* PCS

Figure 2 shows the FTIR spectra and the curve fitting of the secondary protein of GSH and NPTs in *Cladophora* at various Pb concentrations. The peaks shifted from 1653.78 cm⁻¹ to 1633.65 cm⁻¹ and 1651.88 cm⁻¹ after treating *C. rupestris* with Pb^{2+} at concentrations of 1.0 and 5.0 mg/dm³, respectively. This phenomenon was largely caused by C=O stretching vibration. Pb^{2+} was speculated to be complexed with the C=O group to form Pb–C=O. The peak shift at 1560.17 cm⁻¹ was primarily assigned to the stretching vibration of N–H and C–N, indicating that Pb^{2+} combined with the N–H and C–N groups in GSH [7]. The superimposed absorption peak of C–O and O–H at 1261.22 cm⁻¹ shifted to 1256.75 cm⁻¹ and 1256.05 cm⁻¹ under 1.0 and 5.0 mg/dm³ Pb^{2+} stress, respectively. This finding was also attributed to the stretching vibration of C–S [7]. The preceding results indicated that Pb^{2+} complexed with C–O, O–H, and C–S in the GSH of *C. rupestris* to form C–Pb and Pb–C–S structures. The absorption peak at

1026.12 cm^{-1} corresponded to the –COOH group, and the shift in peak position under Pb^{2+} stress could be due to the complexation of Pb and –COOH to form the Pb–C =O structure [14, 15]. Therefore, the FTIR analysis suggested that the GSH of *C. rupestris* played a role by forming Pb–C =O, C–Pb, Pb–COOH, and Pb–C–S combinations.
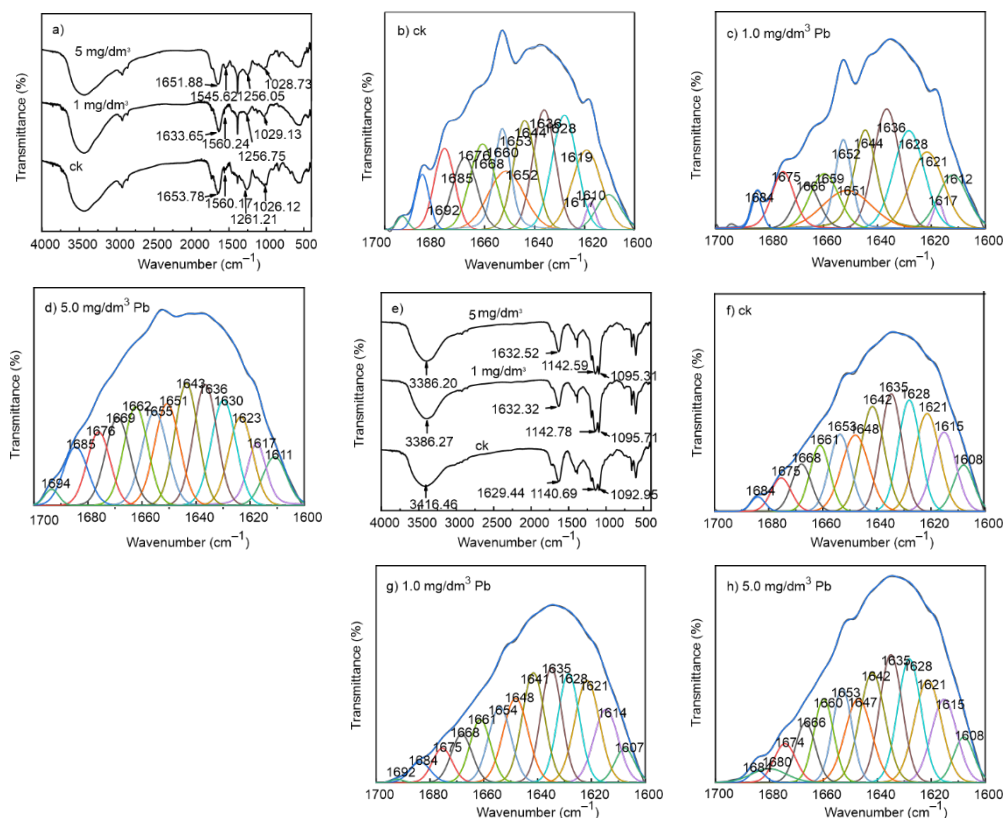

Fig. 2. FTIR analysis and its curve fitting of protein secondary of GSH (a–d) and NPT (e–h) in *Cladophora* at various Pb concentrations

Figure 2e shows the FTIR spectra of NPTs under 1.0 and 5.0 mg/dm^3 Pb^{2+} stresses, respectively. The peak of 3416.46 cm^{-1} displayed a blueshift, indicating that Pb^{2+} bonded with H in NPTs [9]. The peak of 1629.44 cm^{-1} redshifted to 1632.32 cm^{-1} and 1632.52 cm^{-1} under 1.0 and 5.0 mg/dm^3 Pb^{2+} stresses, respectively indicated that C=O combined with Pb to form Pb–C–O [7].

The absorption peak at 1140.69 cm^{-1} that corresponded to the –COOH and C=C groups [7] blueshifted from 1140.69 cm^{-1} to 1142.78 cm^{-1} and 1142.59 cm^{-1} and from 1092.95 cm^{-1} to 1095.71 cm^{-1} and 1095.31 cm^{-1}, indicating that Pb^{2+} complexed with –COOH and C=C to form a more stable structure [20].

Second derivative analysis and curve-fitting procedure were employed to analyze the FTIR spectra ranging from 1700 cm to 1600 cm^{-1}, as shown in Figs. 2b–d and f–h. The relative concentrations of α-helix (1650–1660 cm^{-1}), β-sheet (1600–1640 cm^{-1}), β-turn (1660–1700 cm^{-1}), and random coil (1640–1650 cm^{-1}) [17] are listed in Table 1. The area percentage of each subpeak is the relative content of the secondary protein structure that it represents [18].

Table 1

Relative area percentage ratio of the secondary structure of the protein of GSH and NPT at various concentrations

PCs	Concentration [mg/dm^3]	β-sheet (1600–1640 cm^{-1})	Random coil (1640–1650 cm^{-1})	α-helix (1650–1660 cm^{-1})	β-turn (1660–1700 cm^{-1})
GSH	control	40.89	11.35	18.32	29.44
	1.0	50.19	12.14	24.21	13.46
	5.0	39.25	11.01	19.21	30.53
NPT	control	49.81	24.61	8.84	16.74
	1.0	48.19	24.30	9.10	18.41
	5.0	48.78	23.03	15.78	12.41

The GSH and NPTs of the protein amide I bands of *C. rupestris* have 12–14 sub-peaks in the spectrum, which are attributed to the stretching vibration of C=O, indicating that a complexation reaction occurs between Pb^{2+} and –COOH [18]. The measure of the degree of protein structure looseness and the related groups in NPTs bound to Pb^{2+} making the protein structure more condensed (Table 1). 13 sub-peaks were observed in the NPTs of protein amide I bands under Pb^{2+} stress, and α-helix content in NPTs increased significantly. This finding indicated that NPT chelated with Pb^{2+}, resulting in changes in the protein structure [19]. NPTs and GSH in *C. rupestris* exposed many functional group structures; Pb^{2+} bound with the PCs of *C. rupestris* in Pb^{2+} accumulation, forming a large number of Pb-N protein structures for detoxification [10].

Figure 3 shows the C 1s, N 1s, O 1s, S 2p, and Pb 4f spectra for NPTs and GSH. Figure 3a depicts C 1s spectrum of NPTs. When the concentration of Pb stress was 1.0 and 5.0 mg/dm^3, the peak of the C 1s spectrum was due to C–C at 284.8 eV, C–O/C–N at 286.4 eV, and C=O at 287.9 eV [20]. The peak at 286.4 eV was larger than the three other peaks, indicating that Pb^{2+} was mostly present in C–O/C–N format in NPTs. Lu et al. [21] reported that producing phytochelating peptides could alleviate the toxicity of HMs to plant cells. Therefore, C–O–Pb and Pb–C=O conjugations could be formed in NPTs under Pb stress. The O 1s spectrum belonging to 531.1 eV that was attributed to the –OH bond appeared under Pb^{2+} stress, indicating that the Pb^{2+} and –OH groups exhibited a strong interaction, and –OH was involved in the adsorption of Pb^{2+} [22], and thus, Pb–OH might be formed in NPTs. The N 1s spectrum was divided into four and three peaks when the concentration of Pb stress was 0.5 and 5.0 mg/dm^3, respectively.
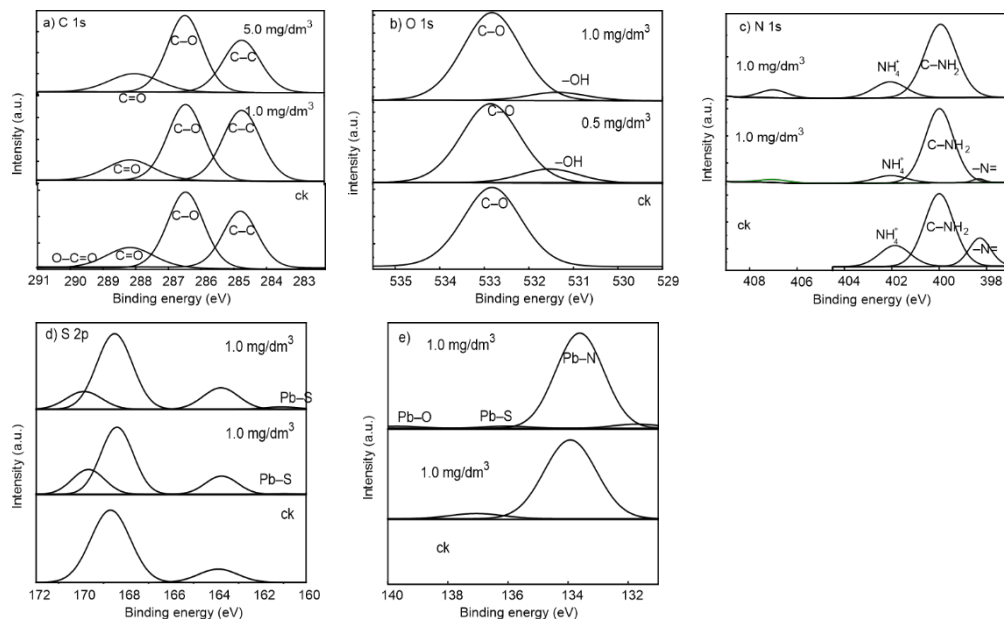
Fig. 3. C 1s，N 1s，O 1s, S 2p, and Pb 4f spectra for the NPT

The maximum at 401.6 eV belonged to the –NH$_4^+$ group, and at 400 eV was probably due to the C–NH$_2$ bond, which was attributed to the adsorbing organic N group. The maximum at 398.3 eV was largely attributed to the –N= group, and –NH$_4^+$ was higher than the control, indicating that –N= and –NH$_4^+$ might chelate with Pb^{2+} to form organometallic complexes. Figure 3d shows the S 2p spectrum at various Pb concentrations in NPTs. The two new peaks at around 161.0 eV and 169.8 eV belonged to Pb–S [23]. The peak at 163.9 eV shifted to 163.7 eV, assigned to C–S, under Pb stress, and Pb^{2+}–C–S complexes were formed. Figure 3e shows the Pb 4f spectra of the NPTs of *C. rupestris* under 1.0 and 5.0 mg/dm^3 Pb stresses. The two peaks that appeared at 133.6 and 137.2 eV were attributed to Pb–O Pb–N and Pb–S in the NPTs of *C. rupestris* under Pb stress [23]. Therefore, the combined forms of Pb^{2+} are mostly Pb–OOC-, Pb–C=O-, C–O–Pb-, Pb–N-, Pb–NH$_2$-, Pb–OH-, and Pb–S-containing complexes in the NPTs of *C. rupestris*.

The XPS spectrum of GSH is shown in Fig. 4. The peaks at 284.8, 287.8, and 289.2 eV in C 1s could be attributed to the increase in C–C, C=O, and O–C=O bonds [24] under Pb stress. The C–O/C–N group at 286.4 eV appeared under 5.0 mg/dm^3 Pb stress, indicating that the C–C group in GSH was chelating with Pb. The strength of the C=O and COO groups in GSH decreased, and thus, the C–O–Pb, C=O–Pb, and Pb–COO complexes were determined to be generated in GSH. Moreover, 399.79 eV moved to 399.98 eV, while 401.9 eV moved to 402 eV; this result was mostly attributed to the C–N group [20].
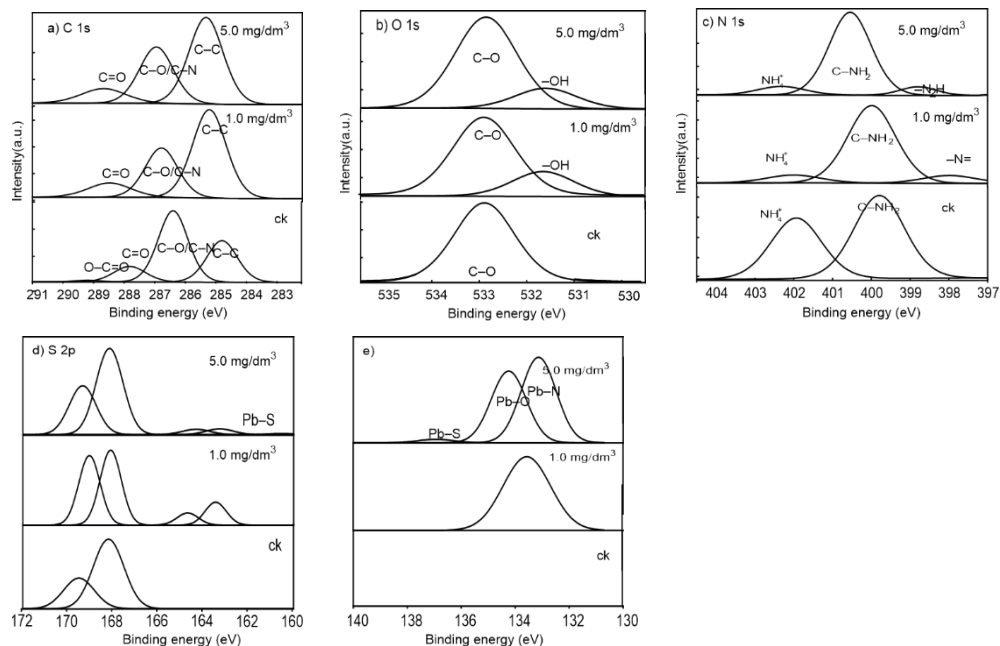
Fig. 4. C 1s，N 1s，O 1s, S 2p, and Pb 4f spectra for the GSH

A new peak at 397.98 eV assigned to the –N= group [24] appeared, indicating that the N-containing groups in GSH bound to Pb^{2+}, and –N=Pb and Pb–NH$_2$ structures might be formed. Some pieces of evidence suggested that GSH/MT and –OH could help Pb^{2+} enter cells. Fig. 4d shows that the Pb–S group appeared when Pb concentration was 5.0 mg/dm^3. The S 2p spectrum exhibited the signal of S– and O-containing species, which might be involved in the absorption of Pb^{2+}. Therefore, C–O–Pb, C=O–Pb, Pb–COO, Pb–S, –N=Pb, Pb–N, and Pb–S were the dominant forms in GSH under Pb stress. This conclusion was similar to that of Chen [2].

Figure 4e shows that the binding form of Pb^{2+} may contain Pb–O compound, Pb–S-containing complex, Pb–N–, and Pb–C–. When the concentration of Pb stress was 1.0 mg/dm^3, the peak at 137 eV in GSH could be attributed to the formation of Pb–S. Two new peaks appeared at 131.5 eV and 139.4 eV under 5.0 mg/dm^3 Pb stress. Zatsepina et al. [25] showed that 139 eV represented Pb–O compound. A peak that belonged to Pb–N– was found in GSH when Pb concentration was 1.0 mg/dm^3 (Fig. 4e). Three peaks appeared, namely, Pb–N– at 133.1 eV, Pb–O at 134.2 eV, and Pb–S at 136.9 eV when *C. rupestris* was under 5.0 mg/dm^3 Pb stress, demonstrating that a large number of Pb^{2+} and N-containing groups combined with phytochelate peptides to form Pb–N–C at high Pb concentrations [20]. Pb^{2+} binds exclusively to the cysteinyl S-donor atom of GSH via ^1H nuclear magnetic resonance (NMR) spectroscopy [6]. Therefore, C–O–Pb, C=O–Pb, Pb–COO, Pb–S, Pb–N, and Pb–S were the dominant forms of GSH under Pb stress.

3.3. SIMULATION OF Pb ABSORPTION AND DETOXIFICATION BY PCS

Figure 5 shows schematically the mechanisms of Pb^{2+} absorption and detoxification by PCs. In conclusion, phytochelating peptides in *C. rupestris* chelate with Pb^{2+} under Pb^{2+} stress. The combined forms of Pb^{2+} were mostly Pb–OOC–, Pb–C=O–, C–O–Pb–, –N=Pb–, Pb–NH$_2$–, Pb–OH–, and Pb–S-containing complexes in the NPTs of *C. rupestris*.
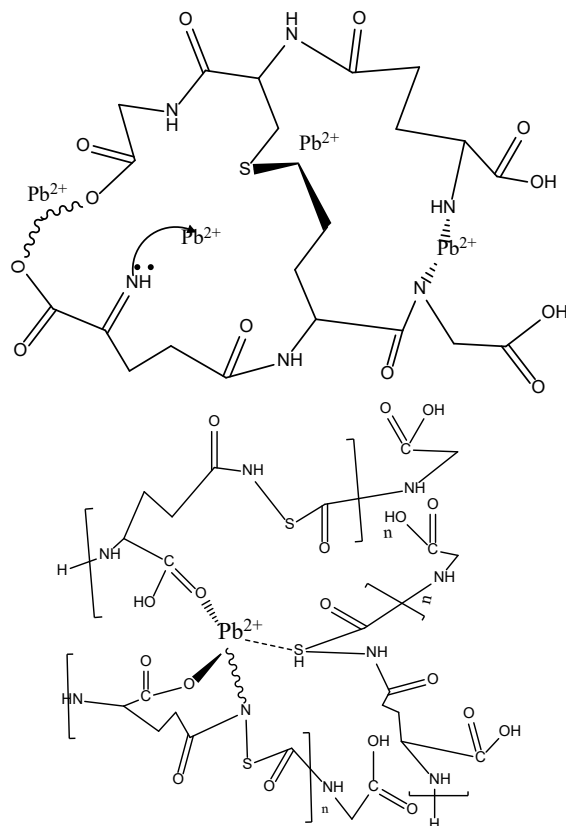

Fig. 5. Pb absorption and detoxification by Phytochelatins

C–O–Pb, C=O–Pb, Pb–COO, Pb–S, and Pb–N were the dominant forms in GSH under Pb stress. GSH chelated to Pb^{2+} ions via their thiol groups, with a similar Pb−S distance of 2.67 Å and a mean Pb−O distance of 2.66 Å [6]. Therefore, complexes that contained Pb–OOC, Pb–C=O, C–O–Pb, –N=Pb, Pb–NH$_2$, Pb–OH, Pb–N–, Pb–C–, Pb–S, and Pb–O compounds were found in the PCs of *C. rupestris*. Complexes Pb(GSH)$_2$ and Pb(GSH)$_3$ with thiolate S atoms formed an asymmetric bridge [6] to reduce the toxicity of intracellular Pb^{2+}. The formulas of GSH and NPTs had no N=, and thus, Pb^{2+} was simulated with two GSHs or NTPs as bridging ligand atoms [17].

4. CONCLUSION

The content of Pb^{2+} in the PCs of *C. rupestris* increased with an increase in Pb^{2+} stress. Pb content increased to 352 and 314 mg/kg in NPTs and GSH, respectively, when Pb stress concentration reached 7.5 mg/dm^3. The Pb^{2+} ratio reached a maximum of 10.8 and 9.3% in NPTs and GSH. The Pb uptake by GSH and NPT was 40–48% and 52–60% in the PCs of *C. rupestris*.

NPTs and GSH in *C. rupestris* revealed many functional group structures. Pb^{2+} bound with the PCs of *C. rupestris* in Pb^{2+} accumulation, forming a large number of Pb–OOC–, Pb–C=O–, C–O–Pb–, –N=Pb–, Pb–NH$_2$–, Pb–OH–, and Pb–S-containing complexes in the NPTs of *C. rupestris*. O–Pb–OH, C–O–Pb, C=O–Pb, Pb–COO, Pb–S, and Pb–N were the dominant forms in GSH under Pb stress. Consequently, Pb^{2+} bound with the PCs of *C. rupestris*, forming complexes that contained Pb–OOC, Pb–C=O, C–O–Pb, –N=Pb, Pb–NH$_2$, Pb–N–, Pb–C–, Pb–S, and Pb–O compounds in PCs to reduce the toxicity of intracellular Pb^{2+}. Pb^{2+} with PCs functioned as bridging ligand atoms. Multiple groups were cross-linked with Pb^{2+} bridges, forming a stable network structure for Pb^{2+} uptake and detoxification in *C. rupestris*.

REFERENCES

[1] NANDA S., KUMAR G., MISHRA R., JOSHI R.K., *Microbe-assisted alleviation of heavy metal toxicity in plants. A review*, Geomicrobiol. J., 2022, 39 (3–5), 416–425. DOI: 10.1080/01490451.2021. 1979697.

[2] CHEN Q.Y., YANG L., LIU L., LI X.X., LI H.D., ZHANG Q., CAO D.J., *XPS and NMR analyze the combined forms of Pb in Cladophora rupestris subcells and its detoxification*, Environ. Sci. Pollut. Res. Int., 2022, 29 (38), 57490–57501. DOI: 10.1007/s11356-022-19880-x.

[3] SHI G.L., LOU L.Q., LI D.J., HU Z.B., CAI Q.S., *Phytochelatins play key roles for the difference in root arsenic accumulation of different Triticum aestivum cultivars in comparison with arsenate uptake kinetics and reduction*, Chemosphere, 2017, 175, 192–199. DOI: 10.1016/j.chemosphere.2017.02.017.

[4] FISCHER S., KUHNLENZ T., THIEME M., SCHMIDT H., CLEMENS S., *Analysis of plant Pb tolerance at realistic submicromolar concentrations demonstrates the role of phytochelatin synthesis for Pb detoxification*, Environ. Sci. Technol., 2014, 48 (13), 7552–7559. DOI: 10.1021/es405234p.

[5] JACQUART A., BRAYNER R., EL HAGE CHAHINE J.M., HA-DUONG N.T., *Cd^{2+} and Pb^{2+} complexation by glutathione and the phytochelatins*, Chem. Biol. Interact., 2017, 267, 2–10. DOI: 10.1016/j.cbi.2016.09.002.

[6] MAH V., JALILEHVAND F., *Lead(II) complex formation with glutathione*, Inorg. Chem., 2012, 51 (11), 6285–6298. DOI: 10.1021/ic300496t.

[7] CHEN Q.Y., YANG L., LIU L., QIAN L.W., TIAN K.L., ZHANG Q., CAO D.J., *Combined forms of Pb and its detoxification and absorption in Cladophora rupestris subcells*, Spectrochim. Acta, A, Mol. Biomol. Spectrosc., 2021, 248, 119190. DOI: 10.1016/j.saa.2020.119190.

[8] CAO D.J., WANG J.J., ZHANG Q., WEN Y.Z., DONG B., LIU R.J., YANG X., GENG G., *Biodegradation of triphenylmethane dye crystal violet by Cedecea davisae*, Spectrochim. Acta, A, Mol. Biomol. Spectrosc., 2019, 210, 9–13. DOI: 10.1016/j.saa.2018.11.004.

[9] CAO D.J., YANG X., GENG G., WAN X.C., MA R.X., ZHANG Q., LIANG Y.G., *Absorption and subcellular distribution of cadmium in tea plant (Camellia sinensis cv. "Shuchazao")*, Environ. Sci. Pollut. Res. Int., 2018, 25 (16), 15357–15367. DOI: 10.1007/s11356-018-1671-5.

[10] CHEN Q.Y., LIU L., YANG L., DONG B., WEN Y.Z., ZHANG Z., ZHANG Q., CAO D.J., *Response of sulfhydryl compounds in subcells of Cladophora rupestris under Pb stress*, Environ. Sci. Pollut. Res. Int., 2021, 28 (11), 13112–13123. DOI: 10.1007/s11356-020-11577-3.

[11] BOUGHRARA L., SEBBA F.Z., SEBTI H., CHOUKCHOU-BRAHAM E., BOUNACEUR B., KADA S.O., ZAOUI F., *Removal of Zn(II) and Ni(II) heavy metal ions by new alginic acid-ester derivatives materials*, Carbohydr. Polym., 2021, 272, 118439. DOI: 10.1016/j.carbpol.2021.118439.

[12] CAO D.J., SHI X.D., LI H., XIE P.P., ZHANG H.M., DENG J.W., LIANG Y.G., *Effects of lead on tolerance, bioaccumulation, and antioxidative defense system of green algae, Cladophora*, Ecotoxicol. Environ. Saf., 2015, 112, 231–237. DOI: 10.1016/j.ecoenv.2014.11.007.

[13] IVANOVA T.M., MASLAKOV K.I., SIDOROV A.A., KISKIN M.A., LINKO R.V., SAVILOV S.V., LUNIN V.V., EREMENKO I.L., *XPS detection of unusual Cu(II) to Cu(I) transition on the surface of complexes with redox-active ligands*, J. Elect. Spectrosc. Rel. Phen., 2020, 238, 146878. DOI: 10.1016/j.elspec.2019.06.010.

[14] LAI H., DENG J., WEN S., LIU Q., *Elucidation of lead ions adsorption mechanism on marmatite surface by PCA-assisted ToF-SIMS, XPS and zeta potential*, Min. Eng., 2019, 144, 106035. DOI: 10.1016/j.mineng.2019.106035.

[15] YU S., SHENG L., MAO H., HUANG X., LUO L., LI Y., *Physiological response of Conyza Canadensis to cadmium stress monitored by Fourier transform infrared spectroscopy and cadmium accumulation*, Spectrochim. Acta, A, Mol. Biomol. Spectrosc., 2020, 229, 118007. DOI: 10.1016/j.saa.2019.118007.

[16] XIE P.P., DENG J.W., ZHANG H.M., MA Y.H., CAO D.J., MA R.X., LIU R.J., LIU C., LIANG Y.G., *Effects of cadmium on bioaccumulation and biochemical stress response in rice (Oryza sativa L.)*, Ecotoxicol. Environ. Saf., 2015, 122, 392–398. DOI: 10.1016/j.ecoenv.2015.09.007.

[17] YANG S., ZHANG Q., YANG H., SHI H., DONG A., WANG L., YU S., *Progress in infrared spectroscopy as an efficient tool for predicting protein secondary structure*, Int. J. Biol. Macromol., 2022, 206, 175–187. DOI: 10.1016/j.ijbiomac.2022.02.104.

[18] SHARMA S., UTTAM K.N., *Investigation of the manganese stress on wheat plant by attenuated total reflectance Fourier transform infrared spectroscopy*, Spectrosc. Lett., 2010, 49 (8), 520–528. DOI: 10.1080/00387010.2016.1212897.

[19] HOU X., LIU S., ZHANG Z., *Role of extracellular polymeric substance in determining the high aggregation ability of anammox sludge*, Water Res., 2015, 75, 51–62. DOI: 10.1016/j.watres.2015.02.031.

[20] LIU X.M., SHENG G.P., LUO H.W., ZHANG F., YUAN S.J., XU J., ZENG R.J., WU J.G., YU H.Q., *Contribution of extracellular polymeric substances (EPS) to the sludge aggregation*, Environ. Sci. Technol., 2010, 44 (11), 4355–4360. DOI: 10.1021/es9016766.

[21] LU Y.J., JIANG A.L., DOU B.R, WANG C., WANG C.H., *Effect of Cd(II) and Zn(II) on growth and biochemical composition of alga Nitzschia closterium*, J. Dalian Fisheries University, 2010, 25 (2), 178–182. DOI: 10.16535/j.cnki.dlhyxb.2010.02.001.

[22] ALI I., PENG C., NAZ I., *Removal of lead and cadmium ions by single and binary systems using phytogenic magnetic nanoparticles functionalized by 3-marcaptopropanic acid*, Chinese J. Chem. Eng., 2019, 27 (4), 949–964. DOI: 10.1016/j.cjche.2018.03.018.

[23] Lai H., Deng J., Wen S., Liu Q., *Elucidation of lead ions adsorption mechanism on marmatite surface by PCA-assisted ToF-SIMS, XPS and zeta potential*, Min. Eng., 2019, 144, 106035. DOI: 10.1016/j.mineng.2019.106035.

[24] Feng Z., Chen H., Li H., Yuan R., Wang F., Chen Z., Zhou B., *Preparation, characterization, and application of magnetic activated carbon for treatment of biologically treated papermaking wastewater*, Sci. Total Environ., 2020, 713, 136423. DOI: 10.1016/j.scitotenv.2019.136423.

[25] Zatsepin D.A., Boukhvalov D.W., Gavrilov N.V., Kurmaev E.Z., Zatsepin A.F., Cui L., Shur V.Y., Esin A.A., *XPS-and-DFT analyses of the Pb 4f –Zn 3s and Pb 5d–O 2s overlapped ambiguity contributions to the final electronic structure of bulk and thin-film Pb-modulated zincite*, Appl. Surf. Sci., 2017, 405, 129–136. DOI: 10.1016/j.apsusc.2017.01.310.